J|A|C|S
ARTICLES

Published on Web 01/26/2010

Structure of $\pi-\pi$ Interactions in Aromatic Liquids

Thomas F. Headen, Christopher A. Howard, Neal T. Skipper,* Michael A. Wilkinson, Daniel T. Bowron, and Alan K. Soper

London Centre for Nanotechnology, Department of Physics and Astronomy, University College London, Gower Street, London WC1E 6BT, United Kingdom, and ISIS Facility, Rutherford Appleton Laboratory, Chilton, Oxfordshire OX11 0QX, United Kingdom

Received October 25, 2009; E-mail: n.skipper@ucl.ac.uk

Abstract: High-resolution neutron diffraction has been used in conjunction with hydrogen/deuterium isotopic labeling to determine with unprecedented detail the structure of two archetypal aromatic liquids: benzene and toluene. We discover the nature of aromatic $\pi-\pi$ interactions in the liquid state by constructing for the first time a full six-dimensional spatial and orientational picture of these systems. We find that in each case the nearest neighbor coordination shell contains approximately 12 molecules. Benzene is the more structured of the two liquids, showing, for example, a sharper nearest neighbor coordination peak in the radial distribution function. Superficially the first neighbor shells appear isotropic, but our multidimensional analysis shows that the local orientational order in these liquids is much more complex. At small molecular separations (<5 Å) there is a preference for parallel $\pi-\pi$ contacts in which the molecules are offset to mimic the interlayer structure of graphite. At larger separations (>5 Å) the neighboring aromatic rings are predominantly perpendicular, with two H atoms per molecule directed toward the acceptor's π orbitals. The so-called "anti-hydrogen-bond" configuration, proposed as the global minimum for the benzene dimer, occurs only as a saddle point in our data. The observed liquid structures are therefore fundamentally different than those deduced from the molecular dimer energy surfaces.

1. Introduction

Aromatic $\pi-\pi$ interactions are now known to play a key role in a wide range of important problems, including the stereochemistry of organic reactions,[1] organic host−guest chemistry and crystal packing,[2−4] protein folding and structure,[5−8] DNA and RNA base stacking,[9] protein−nucleic acid recognition,[10] drug design,[11,12] and asphaltene (heavy crude oil) aggregation and fouling.[13] There has been intensive effort to establish the potential energy surfaces of aromatic molecular dimers. However, detailed knowledge of the structures adopted by simple model aromatic liquids is currently lacking and essential to our fundamental understanding of $\pi-\pi$ interactions in condensed matter. Benzene and toluene are the archetypal aromatic liquids and the simplest molecules with which we can attempt to understand the structures resulting from intermolecular π-orbital interactions. Furthermore, these liquids are extremely important nonpolar organic solvents in their own right and used in a very wide range of laboratory and industrial processes. Toluene is also recognized as one of the molecularly most simple van der Waals glass formers, exhibiting particularly pronounced temperature dependence of the mean reorientation times, a property known as fragility.[14]

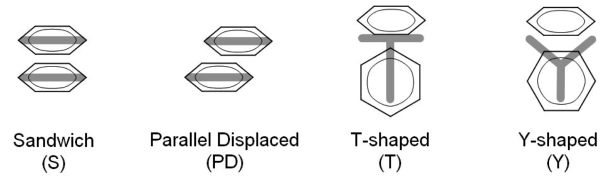

Figure 1. Diagram showing candidate conformations of the benzene dimer: parallel face-to-face "sandwich" (S), parallel displaced (PD), perpendicular T shaped (T), and perpendicular Y shaped (Y).

The delocalized π electrons impart a quadrupolar moment to benzene, toluene, and other aromatic molecules. Favorable electrostatic interactions occur when molecules are either in a parallel (PD) or perpendicular (T or Y) geometry (Figure 1).[15] These electrostatic interactions compete with the attractive

(1) Evans, D. A.; Chapman, K. T.; Hung, D. T.; Kawaguchi, A. T. *Angew. Chem., Int. Ed. Engl.* **1987**, *26*, 1184.
(2) Muehldorf, A. V.; van Engen, D.; Warner, J. C.; Hamilton, A. D. *J. Am. Chem. Soc.* **1988**, *110*, 6561.
(3) Vallée, R.; Damman, P.; Dosière, M.; Toussaere, E.; Zyss, J. *J. Am. Chem. Soc.* **2000**, *122*, 6701.
(4) Ferguson, S. B.; Sanford, E. M.; Seward, E. M.; Diederich, F. *J. Am. Chem. Soc.* **1991**, *113*, 5410.
(5) Burley, S. K.; Petsko, G. A. *Science* **1985**, *229*, 23.
(6) McGaughey, G. B.; Gagné, M; Rappé, A. K. *J. Biol. Chem.* **1998**, *273*, 15458.
(7) Ranganathan, D.; Haridas, V.; Gilardi, R.; Karle, I. L. *J. Am. Chem. Soc.* **1998**, *120*, 10793.
(8) Vondrášek, J.; Bendová, L.; Klusák, V.; Hobza, P. *J. Am. Chem. Soc.* **2005**, *127*, 2615.
(9) Hunter, C. A. *Philos. Trans. R. Soc. London, Ser. A* **1993**, *345*, 77.
(10) Baker, C. M.; Grant, G. H. *Biopolymers* **2007**, *85*, 456.
(11) Frederick, C. A.; Williams, L. D.; Ughetto, G.; van der Marel, G. A.; van Boom, J. H.; Rich, A.; Wang, A. H.-J. *Struct. Biochem.* **1990**, *29*, 2538.
(12) Meyer, E. A.; Castellano, R. K.; Diederich, F. *Angew. Chem., Int. Ed.* **2003**, *42*, 1210.
(13) Marshall, A. G.; Rodgers, R. P. *Acc. Chem. Res.* **2004**, *37*, 53.
(14) Martinez, L. M.; Angell, C. A. *Nature* **2001**, *410*, 663.
(15) Hunter, C. A.; Sanders, J. K. M. *J. Am. Chem. Soc.* **1990**, *112*, 5525.

dispersion forces, which favor maximum molecular contact through a parallel linear "sandwich" (S) orientation.[16] For the benzene dimer, extensive experimental[17−21] and theoretical[22−26] studies have shown that the T and PD configurations are almost isoenergetic but the former (T) is now viewed as the global energy minimum. This T interaction is sometimes referred to as an "anti-hydrogen bond" due to the fact that the donating >C−H bond is shortened.[23] What we will now term a "Y-shaped" configuration, in which two H atoms are directed toward the acceptor aromatic ring, is also found close to the global energy minimum.[22] In the case of toluene, the increased dispersion interactions stabilize the stacked PD geometry[27,28] and the molecular dipole moment favors a staggered (antiparallel) arrangement of the methyl groups over the eclipsed geometry.[10] The crystal structures of benzene[29] and toluene[30−32] are well defined and dominated by the lowest energy dimer motifs, resulting in perpendicular and parallel contacts, respectively. In contrast, there is only very limited experimental diffraction data for the structure of liquid benzene and none in the case of liquid toluene.

Parallel displaced and T-shaped stacking give the most favorable electrostatic interactions, while the sandwich geometry provides the maximum orbital overlap. In the Y-shaped geometry, two H atoms are directed toward the acceptor aromatic ring. For toluene, the lowest energy arrangement for PD places the $-CH_3$ groups antiparallel (staggered) and for T the $-CH_3$ is uppermost.[15,16,22,26]

X-ray and neutron diffraction[33,34] along with optical Kerr effect spectroscopy studies[35] of liquid benzene point toward local ordering that is mostly perpendicular.[36,10] However, without the use of isotopic substitution the neutron diffraction data can only give limited insight into the orientational structure. In response to this lack of conclusive experimental data, a large number of computational studies have been directed toward simple aromatic molecules such as benzene and toluene. Simulations of liquid benzene using classical atom-centered force fields have shown random orientations or a slight preference for perpendicular arrangements of nearest neighbor molecules.[37−39] The use of atom-centered force fields, however, has a drawback in that they do not accurately describe the charge distribution of the aromatic molecule.[15,40] Simulations using partial charges above and below the aromatic ring have attempted to address this issue and for benzene yield a higher preference for perpendicular arrangements of nearest neighbor molecules.[35,41] Liquid toluene has received rather less attention, in spite of the fact that it is viewed as a better model for $\pi-\pi$ interactions in proteins.[42] However, recent simulations indicate a prevalence of parallel stacking of the aromatic planes, with staggered disposition of $-CH_3$ groups.[36,43,10] Since these predictions are highly sensitive to the model force field, high-resolution experimental data are required to guide us.

In this paper a combination of high-resolution neutron diffraction and isotopic substitution of hydrogen for deuterium has been used to determine the detailed structure of liquid benzene and toluene. Data analysis using empirical potential structure refinement (EPSR)[44,45] has allowed us to obtain a full six-dimensional spatial and orientational picture of the liquids and thereby to answer the key questions concerning the nature of aromatic $\pi-\pi$ interactions in these molecular liquids. We find that the nearest neighbor coordination shells contain approximately 12 molecules. When viewed as a whole these shells are orientationally isotropic, but more detailed analysis reveals that the favored nearest neighbor geometry is PD at the smaller separations (<5 Å) and Y shaped at the larger separations (<5 Å). The T-shaped "anti-hydrogen-bond" configuration occurs only as a saddle point.[23] The liquid structures are therefore fundamentally different than those proposed for the molecular dimers.

2. Theory

Hydrogen/deuterium isotopic substitution[46,47] takes full advantage of the very large difference in neutron scattering lengths between hydrogen ($b_H = -3.74$ fm) and deuterium ($b_D = 6.67$ fm). By performing experiments on three samples for benzene and six for toluene in which only the isotopic composition of the hydrogen atoms is varied it is possible for us to obtain reliable radial and orientational structure as the complementary data sets place strong constraints on the structure refinement methods (see section 4).

The quantity measured in a neutron scattering experiment is the differential cross-section.[48] After appropriate corrections this yields the total structure factor, $F(Q)$. We measure M diffraction

(16) Tsuzuki, S.; Honda, K.; Uchimaru, T.; Mikami, M.; Tanabe, K. *J. Am. Chem. Soc.* **2002**, *124*, 104.
(17) Janda, K. C.; Hemminger, J. C.; Winn, J. S.; Novick, S. E.; Harris, S. J.; Klemperer, W. *J. Chem. Phys.* **1975**, *63*, 1419.
(18) Steed, J. M.; Dixon, T. A.; Klemperer, W. *J. Chem. Phys.* **1979**, *70*, 4940.
(19) Law, K. S.; Schauer, M.; Bernstein, E. R. *J. Chem. Phys.* **1984**, *81*, 4871.
(20) Spirko, V.; Engkvist, O.; Soldan, P.; Selzle, H. L.; Schlag, E. W.; Hobza, P. *J. Chem. Phys.* **1999**, *111*, 572.
(21) Ebata, T.; Hamakado, M.; Moriyama, S.; Morioka, Y.; Ito, M. *Chem. Phys. Lett.* **1992**, *199*, 33.
(22) Tsuzuki, S; Honda, K.; Uchimaru, T.; Mikami, M. *J. Chem. Phys.* **2005**, *122*, 144323.
(23) Hobza, P.; Spirko, V; Selzle, H. L.; Schlag, E. W. *J. Phys. Chem. A* **1998**, *102*, 2501.
(24) Hobza, P.; Selzle, H. L.; Schlag, E. W. *J. Phys. Chem.* **1996**, *100*, 18790.
(25) Sinnokrot, M. O.; Sherrill, C. D. *J. Phys. Chem. A* **2006**, *110*, 10656.
(26) Sherrill, C. D.; Takatani, T.; Hohenstein, G. H. *J. Phys. Chem. A* **2009**, *113*, 10146–10159.
(27) Gervasio, F. L.; Chelli, R.; Procacci, P.; Schettino, V. *J. Phys. Chem. A* **2002**, *106*, 2945.
(28) Sinnokrot, M. O.; Sherrill, C. D. *J. Am. Chem. Soc.* **2004**, *126*, 7690.
(29) Jeffery, G. A.; Ruble, J. R.; McCullan, R. K.; Pople, J. A. *Proc. R. Soc. London A* **1987**, *41*, 447.
(30) Andre, D.; Fourme, R. *J. Mol. Struct.* **1982**, *81*, 253.
(31) Anderson, M.; Bosio, L.; Bruneaux-Poulle, J.; Fourme, R. *J. Chim. Phys. Phys. Chim. Biol.* **1977**, *74*, 68.
(32) Ibberson, R. M.; David, W. I. F.; Prager, M. *J. Chem. Soc., Chem. Commun.* **1992**, 1438.
(33) Narten, A. H. *J. Chem. Phys.* **1977**, *67*, 2102.
(34) Misawa, M.; Fukunaga, T. *J. Chem. Phys.* **1990**, *93*, 3495.
(35) Righini, R. *Science* **1993**, *262*, 1386.
(36) Baker, C. M.; Grant, G. H. *J. Chem. Theory Comput.* **2006**, *2*, 947.
(37) Jorgensen, W. L.; Laird, E. R.; Nguyen, T. B.; Tirado-Rives, J. *J. Comput. Chem.* **1993**, *14*, 206.
(38) Jorgensen, W. L.; Maxwell, D. S.; Tirado-Rives, J. *J. Am. Chem. Soc.* **1996**, *118*, 11225–11236.
(39) Cabaco, M. I.; Danten, Y.; Besnard, M.; Guissani, Y.; Guillot, B. *J. Phys. Chem. B* **1997**, *101*, 6977.
(40) Rai, N.; Siepmann, J. I. *J. Phys. Chem. B* **2007**, *111*, 10790.
(41) Zorkil, P. M.; Lanshina, L. V.; Bogdan, T. V. *J. Struct. Chem.* **2008**, *49*, 524.
(42) Chipot, C.; Jaffe, R.; Maigret, B.; Pearlman, D. A.; Kollman, P. A. *J. Am. Chem. Soc.* **1996**, *118*, 11217.
(43) Fioroni, M.; Vogt, D. *J. Phys. Chem. B* **2004**, *108*, 11774.
(44) Soper, A. K. *Chem. Phys.* **1996**, *202*, 295.
(45) Soper, A. K. *Phys. Rev. B* **2005**, *72*, 104204.
(46) Bowron, D. T.; Soper, A. K.; Finney, J. L. *J. Chem. Phys.* **2001**, *114*, 6203.
(47) Soper, A. K. *Chem. Phys.* **2000**, *258*, 121.
(48) Fischer, H. E.; Barnes, A. C.; Salmon, P. S. *Rep. Prog. Phys.* **2006**, *69*, 233.

data sets, $F_i(Q)$, each with a different isotopic composition. The corrected diffraction data is then a weighted sum of the different structure factors arising from the correlations between different pairs of atoms α, β

$$F_i(Q) = \sum_{\alpha,\beta\geq\alpha} (2 - \delta_{\alpha\beta})c_\alpha c_\beta \bar{b}_\alpha \bar{b}_\beta (S_{\alpha\beta}(Q) - 1) \qquad (1)$$

where c_α is the atomic fraction of species α, b_α is the neutron scattering length of atom α, $Q = 4\pi(\sin\theta)/\lambda$ (i.e., the magnitude of the momentum change vector of the scattered neutrons), and $S_{\alpha\beta}(Q)$ is the Faber−Ziman partial structure factor involving atoms α and β only. Equation 1 may be rewritten as

$$F_i(Q) = \sum_{j=1,N} w_{ij}(S_j(Q) - 1) \qquad (2)$$

where $F_i(Q)$ represents the ith data set, the index j runs over the N partial structure factors in the system, and the weights matrix, w_{ij}, is given where j runs over all the N pairs of α,β values. The partial structure factor, $S_{\alpha\beta}(Q)$, contains information about correlations between the two atomic species α and β in Q space and is defined as

$$S_{\alpha\beta}(Q) - 1 = \frac{4\pi\rho_0}{Q}\int_0^\infty r[g_{\alpha\beta}(r) - 1]\sin(Qr)\,dr \qquad (3)$$

where ρ_0 is the atomic number density of the sample and $g_{\alpha\beta}(r)$ is the partial distribution function for the relative density of atoms of type β as a function of their distance, r, from one of type α

$$g_{\alpha\beta}(r) = \frac{\rho_{\alpha\beta}(r)}{\rho_\beta} \qquad (4)$$

This is related to the cumulative coordination number of species β from species α at a distance r by $N(r)$

$$N_{\alpha\beta}(r) = \int_0^r \rho_\beta g_{\alpha\beta}(r)4\pi r^2\,dr \qquad (5)$$

3. Experimental Methods

Diffraction data were collected at the Small Angle Neutron Diffractometer for Amorphous and Liquid Samples (SANDALS) at the ISIS spallation neutron source at the Rutherford Appleton Laboratory, U.K.[49,50] SANDALS is optimized for the measurement of the structure of light element containing disordered systems and in particular for the performance of hydrogen/deuterium substitution measurements.[46] Neutron diffractions of three isotopically distinct samples of benzene and six of toluene were measured at 20 °C. The relative weightings of the individual partial structure factors in these composites depend on the relative concentration and neutron scattering power of the individual atomic species involved (eq 2). The weighting for each atom pair of each sample is shown in Table 1 for benzene and Table 2 for toluene.

The liquids were prepared and inserted into a flat-plate null scattering titanium/zirconium alloy cell with 1 mm thick sample space and wall and mounted onto the instrument's automatic sample changer. This geometry minimizes multiple scattering and absorption effects. The temperature of the samples was maintained to an accuracy of ±0.1 °C using a water bath. Typical counting times were ∼8 h for each sample. For data correction and calibration, scattering data were also collected from the empty instrument (with and without the empty sample cell) and an incoherent scattering vanadium standard slab of thickness 3.0 mm. Background, multiple scattering, absorption, and normalization correction procedures were implemented by the Gudrun suite of programs[49,50] to give the differential scattering cross-section for each isotopically distinct sample. For all samples the "top hat deconvolution" method was used to remove to inelastic self-scattering.[51]

Table 1. Weights Matrix for Our Three Isotopically Distinct Benzene Samples, Calculated Using Eq 2[a]

	D_6-benzene	H_6-benzene	50:50 mix D_6:H_6 benzene
H−H	0.11126	0.03495	0.00537
H−C	0.22168	−0.12425	0.04872
C−C	0.11042	0.11042	0.11042

[a] The weights show how strongly each partial structure factor contributes to the diffraction data.

4. Empirical Potential Structural Refinement Analysis

The technique of empirical potential structural refinement (EPSR) aims to maximize the information that can be extracted from a set of diffraction experiments on a disordered system.[44,45] This method produces a 3-dimensional ensemble of particles which is consistent with the measured diffraction data. The technique uses the diffraction data as a constraint against which to refine a classical molecular simulation of the system under study. The method starts with an equilibrated Monte Carlo configuration based on initial 'seed' potentials. The procedure then iteratively modifies these potentials until the molecular ensemble becomes consistent with the diffraction data. The technique allows known prior information, such as molecular geometry, overlap, and electrostatic constraints, to be built into the refinement procedure.

EPSR simulations were carried out on the data using the six sets of diffraction data for toluene and three for benzene. For both systems the EPSR ensemble consisted of 300 molecules, corresponding to a cubic box of side length 35.4 Å for benzene and 37.7 Å for toluene. The 'seed' potentials used in the refinement were the atom-centered OPLS force field parameters.[36,37] The intermolecular potential includes both the classical Lennard−Jones pairwise potentials and effective charge Coulomb potentials. Bonds are represented by a harmonic potential.[45] Bond angles and dihedrals were maintained by adding harmonic bonds between the first and the third and the first and the forth nearest atoms. For the model of toluene the methyl group was allowed to freely rotate around the >C−CH_3 bond.

The molecular distributions resulting from the EPSR atomic configurations were visualized via a spherical harmonic expansion for the molecular pair correlation functions.[44,47] The spherical harmonic coefficients are calculated from the atomic coordinates every 5 EPSR iterations and then averaged over ∼1000 configurations. The spherical harmonic coefficients can then be used to calculate 3-dimensional atom-centered spatial density plots and to investigate the relative orientations between molecules as a function of their separation. Furthermore, it allows calculation of ring-center to ring-center radial distribution functions. Checks were performed to examine the role of the seed potential on the EPSR by the following. (i) Running EPSR without refinement, i.e., just a Monte Carlo simulation. This allows us to ascertain how the refinement to the data has changed the liquid structure (we will later illustrate this point in Figure 6d). (ii) Using the charge-separated OPLS-CS potential as the seed potential to check the influence of the seed potential on

(49) Soper, A. K.; Howells, W. S.; Hannon, A. C. Atlas-Analysis Time-of-Flight Diffraction Data from Liquid and Amorphous Samples. Rutherford Appleton Laboratory Report RAL-TR-98-006; 1998.
(50) Benmore, C.; Soper, A. K. The SANDALS Manual. Rutherford Appleton Laboratory Technical Report RAL-TR-89-046; 1998.
(51) Soper, A. K. *Mol. Phys.* **2009**, *107*, 1667.

Table 2. Weights Matrix for Our Six Isotopically Distinct Toluene Samples, Calculated Using Eq 2[a]

	H_8-toluene	D_3-toluene	D_5-toluene	D_8-toluene	50:50 mix D_3:D_8 toluene	50:50 mix D_5:D_8 toluene
$H_{Me}-H_{Me}$	0.00559	0.01780	0.00559	0.01780	0.01780	0.000859
$H_{Me}-C_{Me}$	−0.00662	0.01182	−0.00662	0.01182	0.01182	0.00259
$H_{Me}-C_{Me}$	−0.03976	0.07094	−0.03976	0.07094	0.07094	0.01559
$H_{Me}-H$	0.01864	−0.03325	−0.03325	0.05934	0.01304	0.01303
$C_{Me}-C_{Me}$	0.00196	0.00196	0.00196	0.00196	0.00196	0.00196
$C_{Me}-C$	0.02356	0.02356	0.02356	0.02356	0.02356	0.02356
$C_{Me}-H$	−0.01104	−0.01104	0.01971	0.01971	0.00433	0.01971
C−C	0.07067	0.07067	0.07067	0.07067	0.07067	0.07067
C−H	−0.06627	−0.06627	0.11822	0.11822	0.02598	0.11822
H−H	0.01553	0.01553347	0.04945	0.04945	0.002387	0.04945

[a] The weights show how strongly each partial structure factor contributes to the diffraction data. D_3-Toluene is α,α,α-D_3-toluene (only methyl hydrogen deuterated). D_5-Toluene is 2,3,4,5,6-D_5-toluene (only ring hydrogen deuterated). Me subscript is for methyl hydrogen/carbon.

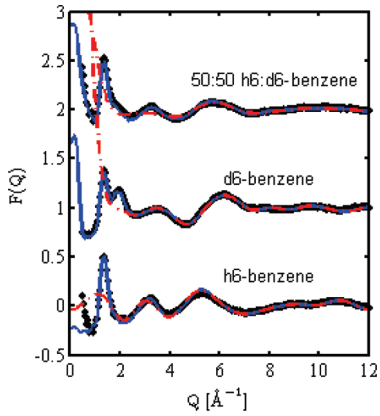

Figure 2. Diffraction pattern (diamonds), EPSR fitted diffraction pattern (blue line), and fitted intramolecular form factor (dashed red line) for different isotopic substitutions of benzene. Note that at higher Q values (>6 Å^{-1}) the scattering is almost exclusively due to the intramolecular correlations.

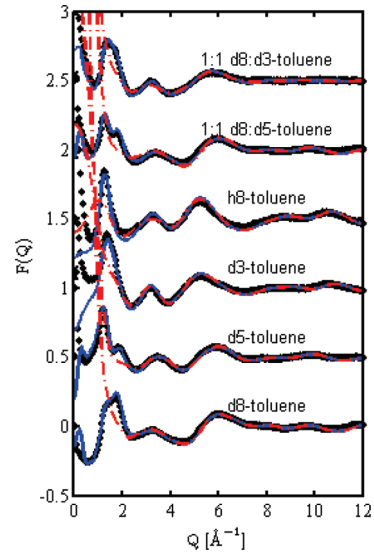

Figure 3. Diffraction pattern (diamonds), EPSR fitted diffraction pattern (blue line), and fitted intramolecular form factor (dashed red line) for different isotopic substitutions of toluene. Note that at higher Q values (>6 Å^{-1}) the scattering is almost exclusively due to the intramolecular correlations.

the structure observed. The OPLS-CS model involves more potential parameters (24 charge sites as compared to 12 for OPLS-AA),[36,37] but its use as a seed did not improve the EPSR fit to our experimental data. We note that the unrefined OPLS-CS model predicts a larger preference for perpendicular neighbors but that EPSR drove the structure to one that was very similar to that obtained from our OPLS-AA seeded refinement which we present in section 5. (iii) Changing the number of dihedrals in the molecules to see how molecular flexibility changes the fit to the data. The best fit to our experimental data was obtained by constraining all intramolecular dihedrals.

5. Results and Discussion

The total normalized structure factors for the three benzene samples and six toluene samples are shown in Figures 2 and 3 together with the EPSR fits. Data were collected over the Q range of 0.125 Å^{-1} < Q < 50 Å^{-1} but are only plotted out to Q = 12 Å^{-1} to allow us to see the salient features more clearly. The agreement between the experimental and fitted data is excellent. The small discrepancies at very low Q are due to the known effects of the inelastic scattering correction in this region.[51] This is confirmed by the observation that a better fit is achieved for the deuterated samples, which suffer less from this effect. Calculation of the purely intramolecular contribution to the $F(Q)$ for each sample is shown as a dashed curve,and confirms that at higher Q values (>6 Å^{-1}) the scattering is almost exclusively due to intramolecular correlations. At the lower Q values, on the other hand, there is strong scattering due to the intermolecular correlations.

Figure 4 shows the benzene ring-center−ring-center (RC−RC), toluene RC−RC, and toluene methyl carbon−methyl carbon (MC−MC) radial distribution functions, $g(r)$ (eq 4), and the cumulative coordination number, $N(r)$ (eq 5). It can be seen immediately that liquid benzene is more structured than toluene owing to the sharper first peak in the $g(r)$. The two liquids show a nearest neighbor coordination shell from approximately 4.0 to 7.5 Å in benzene and 4.0 to 8.0 Å in toluene with maxima at 5.75 Å. These last values compare with center-to-center distances of 3.9 and 5.0 Å for PD and T-shaped benzene dimers, respectively.[26] The coordination numbers in the nearest neighbor shells are approximately 12 molecules for both benzene and toluene, in excellent agreement with previous data.[32−39] The toluene MC−MC $g(r)$ shows a marked nearest neighbor peak in the range 3.5−4.5 Å, with a maximum at 4.15 Å and coordination number of around 1.5 between these two distances. However, it is unclear at this stage whether this feature is caused by methyl−methyl interactions or simply results from packing considerations induced by contacts between the aromatic rings.

In order to further investigate the three-dimensional structure of the respective first coordination shells, spatial density functions (SDFs) of the ring-center correlations have been

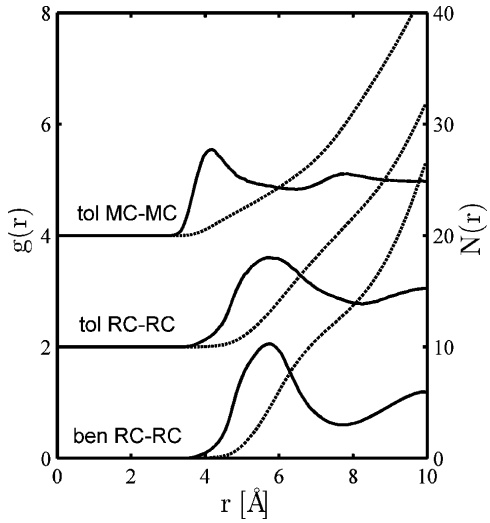

Figure 4. Partial distribution function, $g(r)$ (eq 4), and cumulative coordination number, $N(r)$ (eq 5), for benzene ring-center−ring-center (RC−RC), toluene RC−RC, and toluene methyl-carbon−methyl-carbon (MC−MC) calculated from the EPSR model system. The RC−RC nearest neighbor coordination numbers are approximately 12 for both benzene and toluene. The maxima in the $g(r)$s occur at 4.15 (tol MM−MC), 5.75 (tol RC−RC), and 5.75 Å (ben RC−RC).

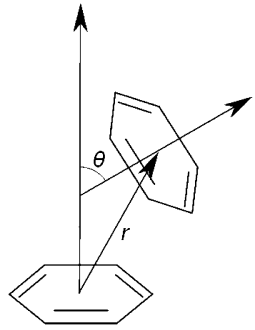

Figure 5. Diagram showing the definition of θ, the minimum angle between the normals to the aromatic planes. Parallel orientations are defined by $\theta \approx 0°$ ($\pm 10°$) and perpendicular orientations by $\theta \approx 90°$ ($\pm 10°$).

calculated. The SDFs show the most probable positions for neighboring molecules around a central reference molecule, which itself is placed in a fixed orientation at the origin. We can further refine this picture by selecting only a particular orientation with respect to the central molecule, for example, to capture aromatic ring planes parallel ($\theta \approx 0°$) or perpendicular ($\theta \approx 90°$) to each other as shown in Figure 5. To visualize such densities we display in three-dimensions the most probable (typically the top 20% or 40%) spatial areas for nearest neighbors.

Figure 6a shows the SDF for nearest neighbor benzene ring-center−ring-center (RC−RC) correlations. From this plot we can immediately identify π-orbital contacts above and below the aromatic ring and also a 6-fold-symmetric "lantern" with a lobe directed toward the center of each C═C bond. We can then further constrain the orientation of both molecules to elucidate the favored geometries. Figure 6b shows the SDF for molecules with aromatic ring planes perpendicular ($\theta \approx 90°$, Figure 5). The density features in this plot are all due to Y-shaped contacts in which two H atoms are either accepted (density above and below) or donated (6-fold lantern lobes) by

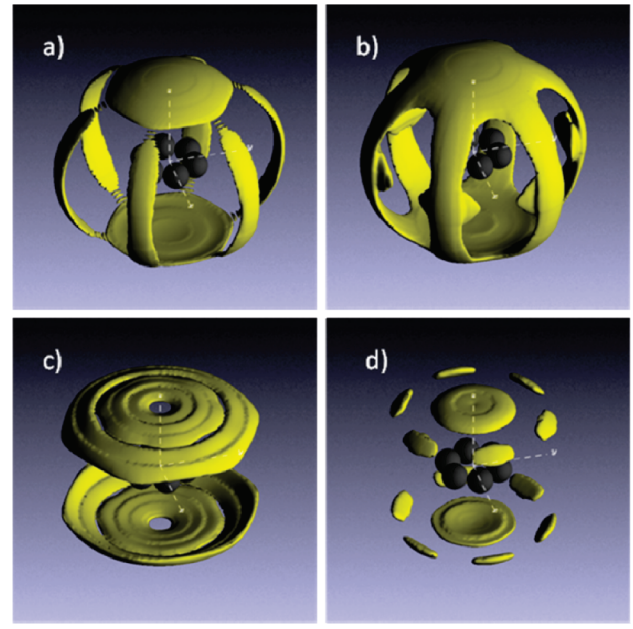

Figure 6. Spatial density functions (SDFs) for liquid benzene showing the most likely positions for molecules in the first coordination shell (2−7.5 Å): (a) The 20% most likely positions for benzene ring-center−ring-center (RC−RC); (b) the 40% most likely positions for benzene RC−RC for perpendicular molecules only, showing predominantly perpendicular Y contacts; (c) the 20% most likely positions for benzene RC−RC for parallel molecules only, showing predominantly parallel PD contacts, and (d) a plot otherwise identical to Figure 6c but now without EPSR refinement to the data, showing face-to-face S contacts.

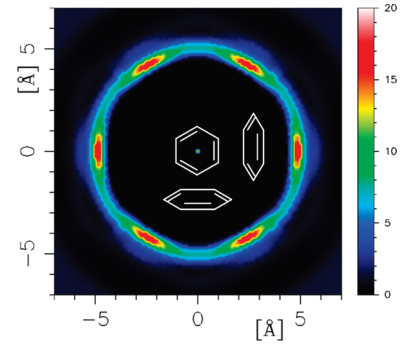

Figure 7. Two-dimensional cut through the spatial density functions (SDFs) for liquid benzene, showing the distribution of first coordination shell (2−7.5 Å) perpendicular molecules around a reference molecule. This projection clearly shows the strong preference for Y-shaped geometries, with T-shaped ones acting as saddle points.

the reference molecule. The latter are illustrated further in the 2-dimensional density projection shown in Figure 7. Note that the T-shaped antihydrogen bonding geometry, derived from ab initio studies of the dimer,[23] appear only as saddle points. We therefore deduce that hydrogen atoms are directed toward the C═C aromatic bond rather than toward the center of the ring. This conclusion is consistent with the observed hydrogen bonding of ammonia to the C═C aromatic bonds in charged fullerene, C_{60}^{5-}.[52,53] Figure 6c shows the SDF for molecules

(52) Howard, C. A.; Thompson, H.; Wasse, J. C.; Skipper, N. T. *J. Am. Chem. Soc.* **2004**, *126*, 13229.
(53) Howard, C. A.; Wasse, J. C.; Skipper, N. T.; Thompson, H.; Soper, A. K. *J. Phys. Chem. C* **2007**, *111*, 5640.

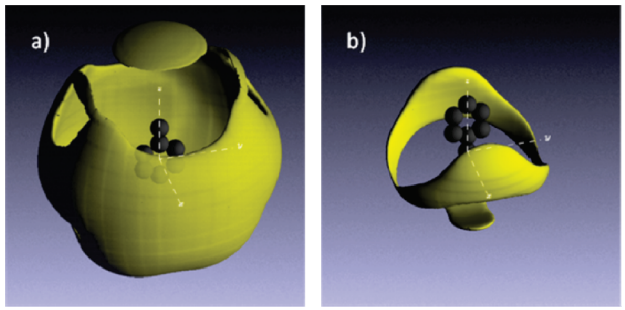

Figure 8. Spatial density functions (SDFs) for liquid toluene showing the most likely positions for molecules in the first coordination shell: (a) the 20% most likely positions for toluene ring-center−ring-center (RC−RC) contacts (2−8 Å) and (b) toluene methyl-carbon−methyl-carbon (MC−MC) contacts (2−5 Å).

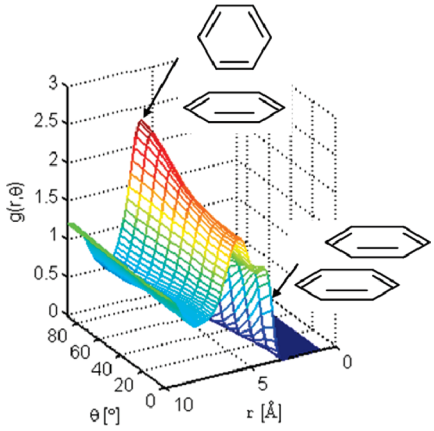

Figure 9. Angular radial distribution function for benzene ring-center−ring-center, $g(r,\theta)$, where θ is the angle between the normals for aromatic planes (see Figure 5). The plot is calculated from our EPSR model system that is refined to the diffraction data and averaged over all directions from the central molecule. The main maximum is at 5.65 Å, and the shoulder seen at 4.25 Å for parallel molecules indicates displaced (PD) $\pi-\pi$ stacking of molecules.

with aromatic ring planes parallel ($\theta \approx 0°$, Figure 5). In this geometry a hole is punched in the density directly above and below each aromatic ring, providing beautiful confirmation that parallel stacking of molecules in the liquid is displaced. In fact, the most popular displacement angle is around 20° and therefore matches that found in graphite. The hole in our SDF corresponds to the absence of sandwich (S) or face-to-face geometry (Figure 1). Figure 6d illustrates powerfully the need for our high-resolution diffraction data in this context, since it shows the SDF derived from the seed potential (i.e., without constraint to the experimental data). This unconstrained SDF shows density directly above and below the aromatic ring, in the sandwich configuration which we now know (from Figure 6c) is inconsistent with the real liquid structure.

The SDF for toluene (Figure 8a) shows considerably less structure than that for benzene due largely to the presence of a symmetry breaking $-CH_3$ group. As with benzene, there is preference for nearest neighbor molecules to be above and below the aromatic core and also for contacts with the aromatic C═C bonds. However, for steric reasons the latter are now concentrated on the four C═C bonds that are furthest from the $-CH_3$ group. As with benzene, the location of these "lantern" density lobes means that two hydrogen atoms must point toward the

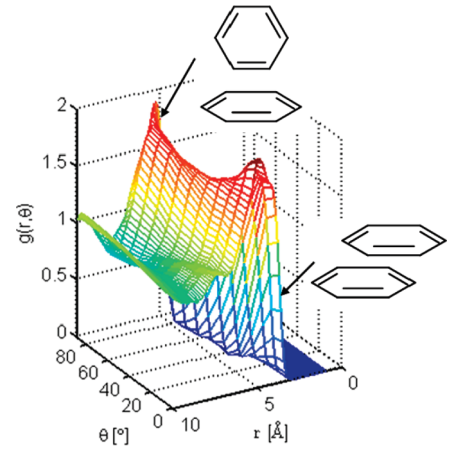

Figure 10. Angular radial distribution function for toluene ring center−ring center, $g(r,\theta)$, where θ is the angle between the normals for aromatic planes (see Figure 6). The plot is calculated from the EPSR model system that is refined to the diffraction data and averaged over all directions from the central molecule. It shows toluene has a very weak preference for parallel arrangements of molecules. The main maximum is at 5.05 Å for $\theta = 0°$ (parallel) and 5.25 Å for $\theta = 0°$ (perpendicular).

accepting aromatic ring to form a Y-shaped configuration rather than an anti-hydrogen-bonded T-shaped geometry. The small cap of density over the $-CH_3$ group is caused primarily by methyl−methyl interactions, which we now address in more detail. Figure 8b shows the SDF for toluene methyl-carbon−methyl-carbon (MC−MC) in the first coordination shell (2−5 Å). The strong lobe under the reference $-CH_3$ group is due to direct MC−MC contacts and gives rise to the concomitant cap in the RC−RC SDF. Please note that we have flipped the reference molecule over in Figure 8b to illustrate this point. The axial strip of density has a strong component above and below the ring but displaced toward the meta and para positions. This is consistent with the PD configuration (Figure 1), with methyl groups arranged antiparallel (staggered) rather than parallel (eclipsed).[43]

The subtleties of the orientational liquid structure can be further investigated by plotting the radial distribution function as a function of the minimum angle between the normals to aromatic planes, as described in Figure 5. This angular radial distribution function, $g(r,\theta)$, is defined in the range $0° \leq \theta \leq 90°$ as

$$g(r,\theta) = \frac{\Delta n(r,\theta)\rho}{4\pi r^2 \sin\theta \cdot \Delta r \cdot \Delta\theta} \qquad (6)$$

where $\Delta n(r,\theta)$ is the number of molecules in the distance range Δr and angle range $\Delta\theta$ and ρ is the bulk number density. The factor $1/(\sin\theta)$ corrects for the well-known dependence of the solid angle on θ when we integrate over azimuthal angle (and which can be seen directly in Figures 11 and 12).

Figures 9 and 10 show the $g(r,\theta)$s for benzene and toluene, respectively. In the case of benzene the $g(r,\theta)$ shows the highest peak for perpendicular arrangements ($\theta \approx 90°$) of molecules: this is the Y-stacked arrangement. In the parallel region (close to $\theta \approx 0°$) we draw attention to the shoulder at $r \approx 4$ Å. This relatively weak feature has to be caused by parallel PD stacking of the aromatic rings: at this low-r distance correlations giving high values of θ simply cannot occur for steric reasons. For toluene the situation is reversed in that the strongest feature can be assigned to parallel displaced stacking. Again we note

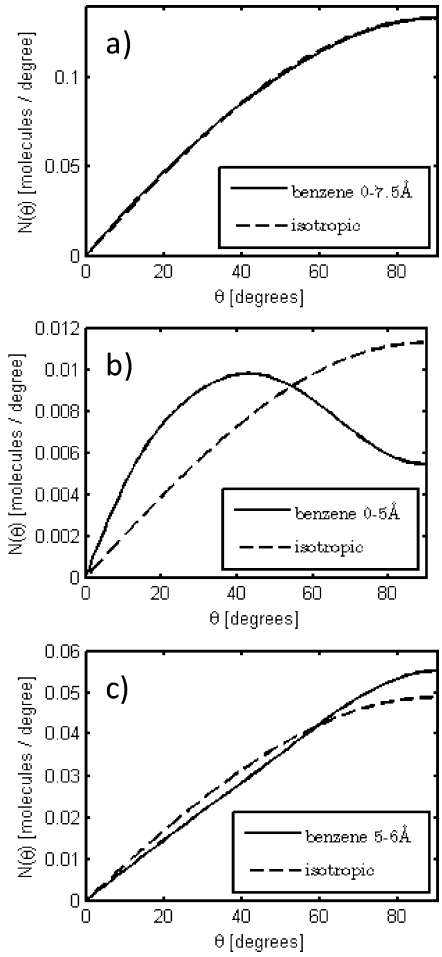

Figure 11. Number distribution of benzene molecules in the first coordination shell as a function of the angle between the aromatic planes, θ (Figure 8). The area under each curve represents the number of molecules in a given angular range for the coordination shells: (a) 0−7.5, (b) 0−5, and (c) 5−6 Å. For reference, the dashed line represents a random isotropic distribution of molecules.

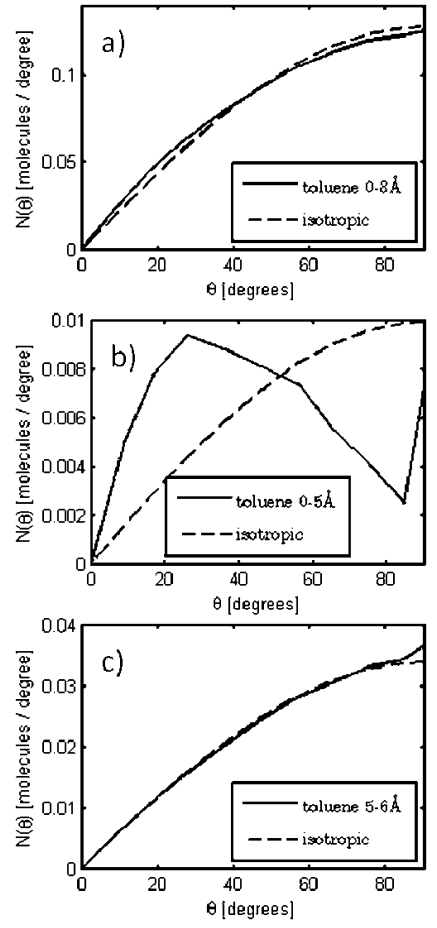

Figure 12. Number distribution of toluene molecules in the first coordination shell as a function of the angle between the aromatic planes, θ (Figure 8). The area under each curve represents the number of molecules in a given angular range for the coordination shells: (a) 0−8.0, (b) 0−5, and (c) 5−6 Å. For reference, the dashed line represents a random isotropic distribution of molecules.

that the nearest neighbor peak in $g(r,\theta)$ shifts to higher r as the molecules rotate to larger θ. This observation leads us to the final question: How anisotropic is the first coordination shell when viewed as a whole?

To answer this question, Figures 11 and 12 plot for benzene and toluene, respectively, the number of first coordination shell molecules as a function of their orientation, θ (Figure 8). For reference, the observed function is compared with a fully isotropic liquid; note again the sin θ dependence we mentioned in the context of eq 6. We see immediately from Figures 11a and 12a that, taken as a whole, the first coordination shells of both benzene and toluene are nearly isotropic. However, at the smaller separations within this shell ($r < 5$ Å) there is a preference for both molecules to exhibit parallel stacking (Figures 11b and 12b). At larger separations ($r > 5$ Å), on the other hand, only benzene shows a marked preference for perpendicular arrangements (Figures 11c and 12c). Thus, in benzene the first coordination shell only appears isotropic because the two anisotropic effects almost cancel each other out.

In complex systems, such as proteins, we would therefore expect the $\pi-\pi$ interactions and resultant stable structures to be either perpendicular (Y) or parallel (PD) depending on the aromatic−aromatic separation. This conclusion is borne out by the pioneering analysis of aromatic groups in protein crystal structures.[5,6] In addition, we already noted that face-to-face π contacts are not observed in our data (see Figure 6c). Remarkably, these configurations were also absent in the above-mentioned proteins.

6. Conclusions

High-resolution neutron diffraction has been used in conjunction with isotopic substitution of hydrogen for deuterium to determine the detailed structure of liquid benzene and toluene. Data analysis using empirical potential structure refinement (EPSR) has allowed us to obtain a full six-dimensional spatial and orientational picture of the liquids and thereby to address the key questions concerning the nature of aromatic $\pi-\pi$ interactions in these molecular liquids. We find that the nearest neighbor coordination shells contain approximately 12 molecules. Benzene is the more structured of the two liquids, showing, for example, a sharper nearest neighbor coordination peak in the radial distribution function. Superficially, the first neighbor shells appear isotropic, but our multidimensional analysis shows that the local orientational order in these liquids is much more complex. At smaller separations the favored nearest neighbor geometry is parallel PD (<5 Å), while at larger

separations (<5 Å) it is perpendicular Y shaped. In the latter, a molecule directs two H atoms toward the aromatic C═C bonds of its neighbor. The T-shaped "anti-hydrogen-bond" configuration, proposed as the global minimum for the benzene molecular dimer,[22,23] occurs only as a saddle point in the liquid state.

Acknowledgment. We are grateful for the support of the UK Natural and Environmental Research Council and the ISIS Neutron Scattering Facility. We thank Professor John Dore for useful discussions.

JA909084E